Truncated singular value decomposition method for calibrating a Stokes polarimeter

Bruno Boulbry,* Jessica C. Ramella-Roman,† and Thomas A. Germer*

*National Institute of Standards and Technology, Gaithersburg, Maryland 20899
†The Catholic University of America, Washington, DC 20064

ABSTRACT

We present a method for calibrating polarimeters that uses a set of well-characterized reference polarizations and makes no assumptions about the optics contained in the polarimeter other than their linearity. The method requires that a matrix be constructed that contains the data acquired for each of the reference polarization states and that this matrix be pseudo-inverted. Since this matrix is usually singular, we improve the method by performing the pseudo-inversion by singular value decomposition, keeping only the four largest singular values. We demonstrate the calibration technique using an imaging polarimeter based upon liquid crystal variable retarders and with light emitting diode (LED) illumination centered at 472 nm, 525 nm, and 630 nm. We generate the reference polarizations by an unpolarized source, a single polarizer, and a Fresnel rhomb. This method is particularly useful when calibrations are performed on field-grade instruments at a centrally maintained facility and when a traceability chain needs to be maintained.

Keywords: calibration, polarimetry

1. Introduction

Mueller-matrix polarimeters (complete polarimeters) or Stokes-vector polarimeters (ellipsometers) have been widely used to measure different polarization properties in optical systems and samples.[1,2] Recently, there have been numerous applications of polarized light including the analysis of polarized light for determining the thickness and refractive index of thin surface films,[3] solar astronomy,[4] remote sensing (underwater surveying, for example[5,6]), telecommunication systems,[7,8] and biology and medicine.[9,10] Imaging polarimetry has also emerged in the last few years to enhance conventional imagery, by providing insightful understanding of the elements that constitute the object based on its polarimetric properties such as birefringence, dichroism, and depolarizing properties.[11,12] Imaging polarimetry is particularly useful to probe the constituent element organization in biological tissues.[13] Spectroscopic polarimeters combine the information available to spectral sensing techniques with polarization.[14] While the spectral information distinguishes materials, polarization information tells us about surface or subsurface features, shape and roughness.[15]

An issue that arises with polarimeters is their proper calibration. Building a Stokes polarimeter with optimal components is often costly, and that cost can often be alleviated by reducing the performance specifications on the components and improving the method by which the polarimeter is calibrated. In this paper, we describe a calibration procedure that makes no assumptions about the components making up the polarimeter other than its linearity and uses reference polarizations that can be traceable to a centrally-maintained reference. The method also yields improved resistance to statistical sources of noise during both the calibration procedure and the subsequent measurement.

This paper is organized as follows. First, in Sec. 2, we review the principles of polarimetry using a data reduction matrix. Next, in Secs. 3 and 4, we describe two methods for calibrating polarimeters, the second one being more general. In Sec. 5, we describe the polarimeter that we use to demonstrate the calibration methods. We then describe a reference polarization generator in Section 6. We present the results for the calibration in Sec. 7. Finally, we summarize our results in Sec. 8.

Polarization Science and Remote Sensing III, edited by Joseph A. Shaw, J. Scott Tyo
Proc. of SPIE Vol. 6682, 66820M, (2007) · 0277-786X/07/$18 · doi: 10.1117/12.734452

2. Principles of measurements

A polarimeter completely or partially measures the Stokes vector of light. The Stokes vector describes the time-averaged polarization properties of an electromagnetic field and is defined as

$$\mathbf{S} = \begin{pmatrix} S_0 \\ S_1 \\ S_2 \\ S_3 \end{pmatrix} = \begin{pmatrix} I_x + I_y \\ I_x - I_y \\ I_{45^\circ} - I_{-45^\circ} \\ I_{\mathrm{lcp}} - I_{\mathrm{rcp}} \end{pmatrix}, \tag{1}$$

where I_j represents the intensity in polarization state j. The subscript j indicates that only that part which is polarized in a particular direction is considered, with lcp and rcp standing for left- and right- circular polarization, respectively. Because of the nature of **S**, the Stokes parameters cannot be measured directly; they must be computed from a set of measurements through polarization analyzers. A straightforward method is to measure four linearly polarized intensities through a linear analyzer at 0°, 45°, 90°, and 135° and through a left- and a right-circular analyzer.[15] The Stokes elements could then be evaluated following the definition of the Stokes vector in Eq. (1). In matrix form, Eq. (1) may be written as

$$\mathbf{S} = \mathbf{W} \cdot \mathbf{I}, \tag{2}$$

where

$$I = \begin{pmatrix} I_x & I_y & I_{45^\circ} & I_{-45^\circ} & I_{lcp} & I_{rcp} \end{pmatrix}^{\mathrm{T}} \tag{3}$$

is a vector containing the six measured intensities, and

$$\mathbf{W} = \begin{pmatrix} 1 & 1 & 0 & 0 & 0 & 0 \\ 1 & -1 & 0 & 0 & 0 & 0 \\ 0 & 0 & 1 & -1 & 0 & 0 \\ 0 & 0 & 0 & 0 & 1 & -1 \end{pmatrix} \tag{4}$$

is referred to as the data reduction matrix. Since

$$I_x + I_y = I_{45^\circ} + I_{-45^\circ} = I_{rcp} + I_{lcp}, \tag{5}$$

the matrix **W** is not unique. For example, the matrix

$$\mathbf{W} = \begin{pmatrix} 1/3 & 1/3 & 1/3 & 1/3 & 1/3 & 1/3 \\ 1 & -1 & 0 & 0 & 0 & 0 \\ 0 & 0 & 1 & -1 & 0 & 0 \\ 0 & 0 & 0 & 0 & 1 & -1 \end{pmatrix} \tag{6}$$

should give equivalent results, provided Eq. (5) holds.[16,17] The sum of the squares of each element in a row determines the relative error propagated from uncorrelated uncertainties in the signal levels to each of the Stokes vector elements.[16,17] In fact, the matrix in Eq. (6) will yield a lower uncertainty for the first Stokes element and can be shown to be an optimal matrix. [16,17]

3. Old Calibration Method

A polarimeter is typically composed of a collection of retarders and polarizers that are cascaded to form a polarization state analyzer. The components are modulated, either by rotating one or more of them or by varying their retar-

dance, and signals are acquired for each of several configurations. The Stokes vector $\mathbf{S}_i$ of the light reaching the detector when the analyzer is in configuration i is

$$\mathbf{S}_i = \mathbf{M}_i \cdot \mathbf{S} \tag{7}$$

where $\mathbf{M}_i$ is the Mueller matrix of the respective analyzer. The measured intensity I_i is the first term of $\mathbf{S}_i$ and can be expressed as a function of the four unknown components,

$$I_i = \mathbf{S}_{\text{sense},i} \cdot \mathbf{S}\,, \tag{8}$$

where we define a Stokes sensitivity vector, consisting of the first row of $\mathbf{M}_i$,

$$\mathbf{S}_{\text{sense},i} = \begin{pmatrix} M_{i,00} & M_{i,01} & M_{i,02} & M_{i,03} \end{pmatrix}. \tag{9}$$

If we define a matrix $\mathbf{A}$ to contain the Stokes sensitivities for each of the configurations of the polarimeter, then the intensity vector for an unknown Stokes vector is

$$\mathbf{I} = \mathbf{A} \cdot \mathbf{S}\,, \tag{10}$$

where

$$\mathbf{A} = \begin{pmatrix} M_{1,00} & M_{1,01} & M_{1,02} & M_{1,03} \\ \vdots & \vdots & \vdots & \vdots \\ M_{N,00} & M_{N,01} & M_{N,02} & M_{N,03} \end{pmatrix}. \tag{11}$$

Finally, we can then find $\mathbf{W}$ by solving for $\mathbf{S}$ in Eq. (10). That is, $\mathbf{W}$ is given by the pseudo-inverse of $\mathbf{A}$:

$$\mathbf{W} = (\mathbf{A}^{\mathrm{T}} \cdot \mathbf{A})^{-1} \cdot \mathbf{A}^{\mathrm{T}}\,. \tag{12}$$

Unfortunately, this method requires each of the Stokes sensitivities [Eq. (11)] to be known. A conventional method to calibrate such a system is to assume a parameterization for each optical element. For example, for a retarder, one will assume it is fully characterized by a retardance and an orientation. A regression analysis is then performed on a set of calibration data. Optical devices and their physical orientation, however, are never perfect. Some physical effects, such as multiple reflections between or within optical devices, incorrectly oriented crystals in retarders, imperfect polarizers, and residual birefringence, will often cause the Mueller matrices of the analyzer components to deviate from the ideal, and moreover, will cause them to deviate from what has been parameterized.[18,19] For field instruments, obtaining high quality components to alleviate these concerns adds to their price, substantially.

4. New Calibration Method

In this section we describe a procedure that can be used to calibrate any Stokes polarimeter, without requiring knowledge of the details of the components making up that polarimeter. We assume that the polarimeter measures N intensities corresponding to the N different configurations of the analyzing elements. The matrix $\mathbf{W}$ is thus of dimension $4\times N$. To calibrate the polarimeter, let us assume we can generate M different reference polarization states, for which we know the Stokes vectors $\mathbf{S}_i$ ($i = 1,\ldots, M$). We thus know that

$$\begin{bmatrix} \mathbf{S}_1 & \mathbf{S}_1 & \ldots & \mathbf{S}_M \end{bmatrix} = \mathbf{W} \cdot \begin{bmatrix} \mathbf{I}_1 & \mathbf{I}_2 & \ldots & \mathbf{I}_M \end{bmatrix} \tag{13}$$

should hold, where $\mathbf{I}_i$ is the vector containing the N measurements for the i-th Stokes vector. We can rewrite Eq. (13) as

$$\mathbf{S} = \mathbf{W} \cdot \mathbf{I}\,, \tag{14}$$

where $\mathbf{S} = [\mathbf{S}_1\ \mathbf{S}_2\ \ldots\ \mathbf{S}_M]$ is a $4\times M$ matrix, and $\mathbf{I} = [\mathbf{I}_1\ \mathbf{I}_2\ \ldots\ \mathbf{I}_M]$ is a $N\times M$ matrix. The data reduction matrix $\mathbf{W}$ can then be determined by pseudo-inverting $\mathbf{I}$:

$$\mathbf{W} = \mathbf{S} \cdot \mathbf{I}^{-1}. \tag{15}$$

The pseudo-inverse of [**I**] can be determined from

$$\mathbf{I}^{-1} = \mathbf{I}^{\mathrm{T}} \cdot \left(\mathbf{I} \cdot \mathbf{I}^{\mathrm{T}} \right)^{-1} . \tag{16}$$

However, one must be careful when using Eq. (16) because the matrix $\mathbf{I} \cdot \mathbf{I}^{\mathrm{T}}$ is not well-conditioned and pseudo-inversion can lead to large variations in the resulting matrix **W**. That is, while **I** is an $N \times M$ matrix, theoretically (in the limit of no measurement errors) it has only 4 non-zero singular values. The variations that occur are a manifestation of the non-uniqueness of **W**, seen above in Eqs. (4) and (6). While the resulting matrix may function as expected, it cannot be easily compared to the ideal matrix, and the uncertainties in subsequent measurements may not be optimized.

A solution to this problem consists of using the singular value decomposition (SVD) to calculate the pseudo-inverse of **I**.[20] The SVD decomposes any matrix **I** into the product of two real orthonormal matrices, **U** (of dimension $N \times N$) and **V** (of dimension $M \times M$), and a diagonal real matrix **D** (of dimension $N \times M$), such that

$$\mathbf{I} = \mathbf{U} \cdot \mathbf{D} \cdot \mathbf{V}^{\mathrm{T}} . \tag{17}$$

By convention, the diagonal elements σ_i of **D**, which are referred to as the singular values of **I**, are non-negative and sorted in decreasing order, i.e., $\sigma_1 \geq \sigma_2 \geq \ldots \geq \sigma_p \geq 0$; this convention makes the SVD unique except when one or more singular values occur with multiplicity greater than one (in which case the corresponding columns of **U** and **V** can be replaced by linear combinations of themselves). An important property of the SVD is that it explicitly constructs orthonormal bases for the range and the nullspace of **I**. Specifically, the columns of **U** whose same-numbered elements σ_i are non-zero are an orthonormal set of basis vectors that span the range; the columns of **V** whose same-numbered elements are zero are an orthonormal basis for the nullspace.[21]

To determine the number of non-zero singular values of **I**, consider that it contains columns consisting of the measured intensities for a set of Stokes vectors having 4 degrees of freedom. It is thus obvious that if the input Stokes vectors span all 4 dimensions, then the range of **I** should have 4 dimensions. Thus, **I** should only have 4 non-zero singular values.

One advantage of the SVD is that the pseudo-inverse of the matrix can be determined from

$$\mathbf{I}^{-1} = \mathbf{V} \cdot \mathrm{diag}(1/\sigma_1, .., 1/\sigma_N) \cdot \mathbf{U}^{\mathrm{T}} . \tag{18}$$

If the matrix is singular, then the inverse of any zero singular value is set to zero. In practice, with random errors introduced into the measurement, the matrix **I** has N non-zero singular values, yet all but 4 of them are very small. We argue that these small singular values should be treated as zero, since otherwise their effect on the pseudo-inverse is very large, yet their significance is negligible. They exist to reproduce the noise in the calibration measurement and to span the space of non-optimal matrices. Thus, we use the truncated pseudo-inverse

$$\hat{\mathbf{I}}^{-1} = \mathbf{V} \cdot \mathrm{diag}(1/\sigma_1, .., 1/\sigma_4, 0, ..., 0) \cdot \mathbf{U}^{\mathrm{T}} \tag{19}$$

and let

$$\mathbf{W} = \mathbf{S} \cdot \hat{\mathbf{I}}^{-1} . \tag{20}$$

As we will demonstrate later, the effect of using the truncated pseudo-inverse is that the data reduction matrix is stable, optimized, and less susceptible to measurement uncertainties.

5. The polarimeter

We have constructed and operated a spectroscopic Stokes polarimeter using a pair of liquid-crystal (LC) devices in combination with a polarizer,[22] shown schematically in the bottom frame of Fig. 1. The LC devices act as uniaxial variable retarders, with their retardance being controlled by an external applied voltage. One of the main interest of using these devices is that they can be switched at near-video-frame rates for imaging applications.[23] In addition, they do not require any moving parts, have large acceptance angles, and large clear apertures.

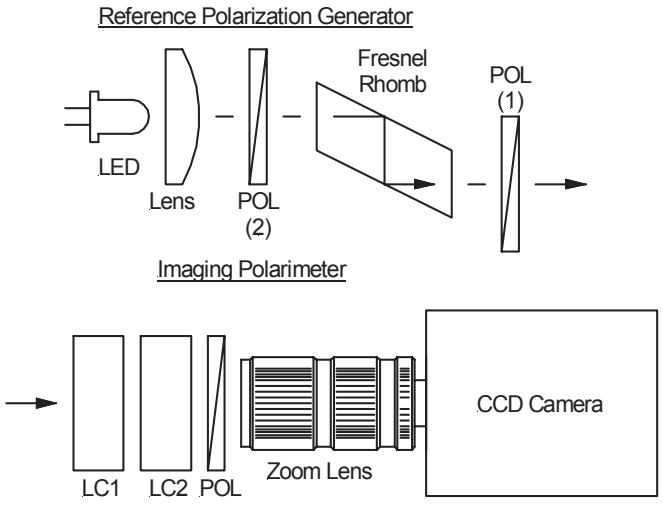

Figure 1. The Reference Polarization Generator (bottom) and the Imaging Polarimeter (top). The polarizer (POL) in the Reference Polarization Generator is placed in positions 1 and 2 for the two configurations.

In our measurements the fast axes of the LC retarders were nominally oriented at the fixed angles $\theta_1 = 0°$ and $\theta_2 = -45°$ with respect to the polarizer, and the nominal retardance combinations were varied according to $(\delta_1, \delta_2) = (0°, 0°)$, $(0°, 180°)$, $(-90°, 90°)$, $(-90°, -90°)$, $(0°, -90°)$, $(0°, 90°)$, leading to the nominal analysis matrix

$$\mathbf{A} = \begin{pmatrix} 1 & 0 & 0 & 1 \\ 1 & 0 & 0 & -1 \\ 1 & 1 & 0 & 0 \\ 1 & -1 & 0 & 0 \\ 1 & 0 & 1 & 0 \\ 1 & 0 & -1 & 0 \end{pmatrix}. \tag{21}$$

The voltages applied to the LC retarders to get the desired retardance were calculated using calibration data provided by the manufacturer. Since the manufacturer only provided data for a single wavelength ($\lambda = 633$ nm), data for other wavelengths were determined by assuming that the devices had no dispersion. Ideally, the Mueller matrix for the analyzer is

$$\mathbf{M} = \mathbf{M}_{\text{pol}}(\theta_3) \cdot \mathbf{M}_{\text{ret}}(\theta_2, \delta_2) \cdot \mathbf{M}_{\text{ret}}(\theta_1, \delta_1), \tag{22}$$

where $\mathbf{M}_{\text{pol}}(\theta)$ is the Mueller matrix for a polarizer at angle θ, and $\mathbf{M}_{\text{ret}}(\theta, \delta)$ is the Mueller matrix for a retarder with retardance δ oriented with its fast axis at angle θ.

The detector consisted of a 12-bit digital charge-coupled device (CCD) camera with a zoom lens. For the calibration of this instrument, a diffuser was placed between the polarizer and the front of the zoom lens, so that the camera was effectively being used as an integrating, non-imaging detector. The signals that were obtained from the camera were averaged over the active area of the detector array.

6. Calibration procedure

The procedures described in Secs. 3 and 4 require that a set of well-defined polarization states be generated and measured by the polarimeter. These states should span all of the dimensions of the Poincaré sphere. Furthermore, it is

advantageous if the intensities for all of the states are the same, or at least calculable *a priori*. In the following we describe a configuration, shown in the top frame of Fig. 1, that is relatively easy to configure in a laboratory and satisfies these requirements.

We begin by generating a source of unpolarized light. We then use a polarizer and a quarter-wave retarder. The polarizer is placed in a rotation stage that in turn can be placed before [(2) in Fig. 1] or after [(1) in Fig. 1] the quarter-wave retarder. The retarder is aligned so that its fast axis is horizontal or vertical, and the polarizer is initially aligned to this direction. The signals measured by the polarimeter are then measured for a number of orientations of the polarizer placed both before and after the retarder. When the polarizer is before and after the retarder, the polarization states are given by

$$\mathbf{S}^{\text{before}}(\theta) = \begin{bmatrix} 1 & \cos 2\theta & 0 & \sin 2\theta \end{bmatrix}^{\mathrm{T}}, \tag{23}$$

and

$$\mathbf{S}^{\text{after}}(\theta) = \begin{bmatrix} 1 & \cos 2\theta & \sin 2\theta & 0 \end{bmatrix}^{\mathrm{T}}, \tag{24}$$

respectively. Because the light incident upon the polarizer is always unpolarized in both configurations, the number of interfaces is constant, and if the retarder has no diattenuation, then the intensities for all of the reference states remain constant. These states also span the Poincaré sphere. Of course, one needs to obtain a sufficiently good source of unpolarized light, a sufficiently good polarizer, and a sufficiently accurate quarter-wave retarder. On the other hand, once one calibrates a well-characterized polarimeter, the polarimetric scale can be transferred to any other polarimeter, using a source which may deviate substantially from the behavior given in Eqs. (23) and (24).

In our implementation, we used a tri-color light emitting diode (LED) as a source. The tri-color LED emits in three bands: red (centered on $\lambda = 630$ nm), green (centered on $\lambda = 525$ nm), or blue (centered on $\lambda = 472$ nm). The widths of the three bands were all about 25 nm, measured full-width at half maximum. The light emitted by the LEDs was found to have no residual polarization.

For the polarizer, we used a dichroic polarizer. These devices can be readily obtained, and many have a very good extinction coefficient (around 10^4 in the visible spectrum[24]). They also have a large open angular aperture and a large angular acceptance. We also have used Glan-style polarizers; the results were comparable but are not presented here. The polarizer was mounted in a manually actuated rotation stage, having a precision of about 1°.

For the retarder, we used a BK7 Fresnel rhomb. These devices are based on the phase shift of total internal reflection between the s- and p- polarized waves and are used as quasi-achromatic quarter-wave retarders.[25] The residual reflection from the faces of the rhomb are not polarization dependent, since the light is incident at normal incidence and the material is not birefringent. These devices exhibit a variation in the maximum of the relative phase of 2% in the visible spectral band. However this phase shift can be easily determined using the Fresnel equations and knowing the Fresnel rhomb's parameters (refractive index and incident angle). Another advantage of Fresnel rhombs is that they do not rely upon accurate crystal orientation for their performance. A disadvantage of the Fresnel rhomb is that it translates the beam by a large amount. This problem is alleviated by the arrangement of the polarizer and the rhomb, whereby it is the polarizer that is rotated during the procedure rather than the rhomb, and the beam path is fixed.

The polarizer is initially aligned with respect to an auxiliary polarizer by finding the angle of maximum extinction. The retarder is then placed between the two polarizers and aligned to re-attain maximum extinction. The axis of the system is thus defined by this auxiliary polarizer. In our measurements, we used the polarizer in the polarimeter (with the LC retarders removed) as the auxiliary reference polarization, but that should have little effect on the results. We measured the intensity for 18 different orientations (10° apart) for each of the two configurations (polarizer-rhomb and rhomb-polarizer), yielding a total of $M = 36$ reference Stokes vectors.

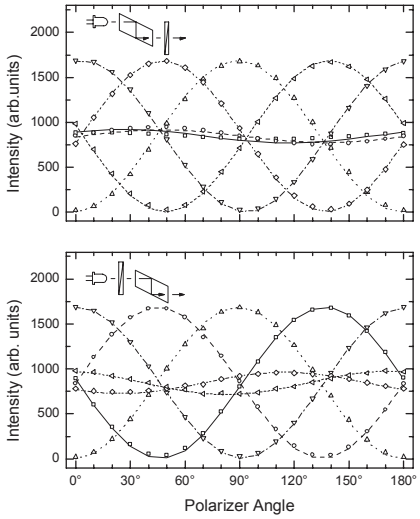

Figure 2. The calibration data (symbols) obtained for λ = 630 nm and the best fit (curves) to the first calibration method. The top frame is for the rhomb-polarizer configuration, and the bottom frame is for the polarizer-rhomb configuration.

Table 1. The best fit parameters obtained from a non-linear least squares fit to the calibration data.

Fitted Parameter	Nominal Value	Wavelength		
		630 nm	525 nm	472 nm
θ_1	0°	2.60°	2.13°	–0.02°
θ_2	–45°	–43.75°	–43.42°	–42.12
θ_3	0°	–0.92°	–1.39°	0.61°
δ_1^a	0°	–0.44°	–0.38°	–0.26°
δ_1^b	–90°	–91.89°	–96.67°	–100.56°
δ_2^a	0°	–1.50°	–0.37°	0.04°
δ_2^b	–90°	–89.81°	–93.82°	–100.87°
δ_2^c	–180°	–177.44°	–189.46°	–202.62°
δ_2^d	–270°	–266.79°	–282.19°	–300.02°

7. Calibration results

Two different methods were used to calibrate the system. In the first method, it was assumed that Eq. (22) was valid, and a non-linear least squares fit of the measured 36×6 intensities was performed allowing the six retardance values ($\delta_1 = \delta_1^a$ and δ_1^b, and $\delta_2 = \delta_2^a$, δ_2^b, δ_2^c, and δ_2^d), the three orientations of the elements (θ_1, θ_2, and θ_3), and an overall intensity to be free parameters. The second method used the algorithm described in Sec. 4, making no assumptions about the Mueller matrices of the polarimeter. These methods were performed for data taken for each of the three different wavelengths.

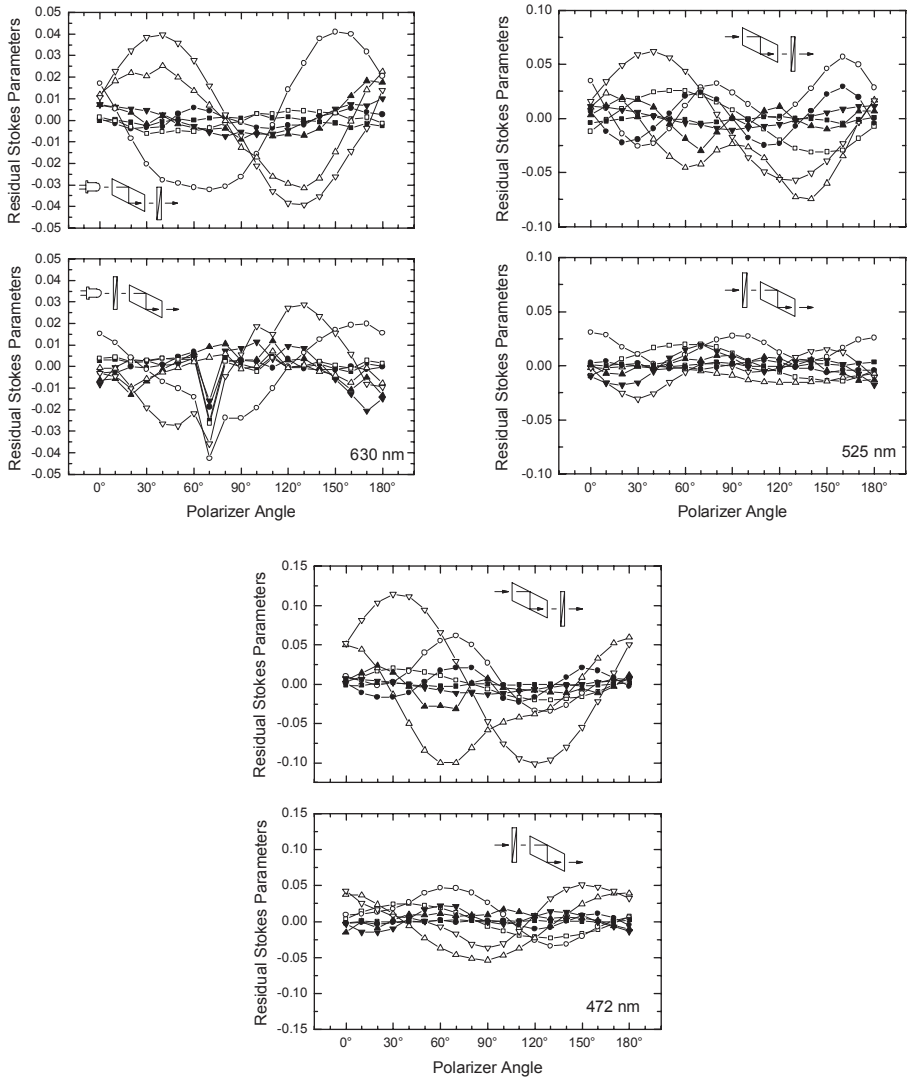

Figure 3. The residual normalized Stokes parameters for (upper left) λ = 630 nm, (upper right) λ = 525 nm, and (lower) λ = 472 nm as a function of polarizer angle. The symbols are (squares) S_0, (circles) S_1, (up triangles) S_2, (down triangles) S_3, (open) the first calibration method, and (solid) the second calibration method. The top frame is for the rhomb-polarizer configuration, and the bottom frame is for the polarizer-rhomb configuration.

Figure 2 shows the resulting best fit to the data for the red LED (λ = 630 nm) using the first method, while Table 1 shows the best fit parameters for all three wavelengths. The data show small deviations from the theory that could not be described by the simplified description of the polarimeter. The orientation angles shown in Table 1 are all consistent with one another (the polarization optics were not moved between the measurements), but have a systematic offset of a couple degrees. The retardances also show systematic variation from their optimum values. These retardances differ from their nominal values partly due to misalignments and non-ideal behavior of the elements, but mostly from the calibration data for the LC modulators being given by the manufacturer at only a single wavelength of 633 nm. Figure 3 shows the residual calibration Stokes vectors calculated by applying the data reduction matrix obtained for all three wavelength to the calibration data. The root mean square (rms) residuals between the reference values and the measured values for all the wavelengths are given in Table 2.

Table 2. Root-mean-square error of the Stokes vector elements based upon the two calibration methods described in the text.

	Wavelength		
	630 nm	525 nm	472 nm
First method	0.020	0.024	0.044
Second method	0.006	0.011	0.011

A data reduction matrix was then calculated using the second method, as described in Sec. 4. Figure 3 shows the calibration Stokes vectors calculated by applying the new data reduction matrices obtained for all three wavelengths to the calibration data. Comparing the results shown in Fig. 3, we see that the resulting Stokes vectors are much closer to their reference values when we use the second method. Again, the rms residuals are given in Table 2. One can see that the second method yields rms residuals lower by at least a factor of 2.

The calibration procedure was repeated five times to demonstrate the consistency in the matrix **W** obtained by the second procedure, using the non-truncated SVD inversion in Eq. (18) and the truncated SVD inversion in Eq. (19). The resulting matrices **W** were compared to the average of the five matrices computed using the truncated SVD inversion. The RMS deviation between the matrices computed by non-truncated SVD inversion was 3.6, much larger than the mean matrix element, while that between the matrices computed by the truncated SVD inversion was 0.06. Thus, while the matrices **W** appeared unrelated to one another when the non-truncated SVD inversion was used, those calculated using the truncated SVD inversion were relatively stable and closer to the nominal matrix given in Eq. (6).

Some of the improvements in the results between the first and second methods may be a result of inaccuracy in the reference Stokes vectors. That is, the second method will force the calibration to match the reference Stokes vectors, even if the reference Stokes vectors are far from ideal. Thus, the method described is expected to yield substantially improved results when a good reference Stokes generator is available, and especially when the polarimeter itself has components that are far from ideal. Such conditions are expected in field instruments that are calibrated at a single facility.

8. Conclusion

An imaging Stokes polarimeter using of a pair of LC variable retarders and a sheet polarizer has been described. The reference polarizations for the polarimeter calibration were generated by an unpolarized source, a polarizer, and a Fresnel rhomb, with the order of the polarizer and rhomb being interchanged. Two calibration analysis procedures were described. In the first case, assumptions were made about the optical elements in the polarimeter, and a regression analysis was used to optimize the parameters. In the second case, no assumptions about the polarimeter were made, but the data reduction matrix was obtained by pseudo-inverting the calibration measurement matrix, where pseudo-inversion was performed by SVD, keeping only the 4 largest singular values. The second method improved the results substantially. This method has advantages, because it can reduce the fabrication requirements of polarimeters and thus reduce their cost.

References

1. R. M. A Azzam, and N. M. Bashara, *Ellipsometry and Polarized light* (New York: North Holland, 1987).
2. R. A. Chipman, "Polarimetry," in *Handbook of Optics* (New York: McGraw-Hill), Vol. 2, Chap. 22 (1995).
3. A. En Naciri, L. Johann, R. Kleim, M. Sieskind, and M. Amann "Spectroscopic ellipsometry of anisotropic materials: application to the optical constants of HgI_2", Appl. Opt. **38**, 647-654 (1999).
4. T. W. Cronin, E. J. Warrant, and B. Greiner, "Celestial polarization patterns during twilight," Appl. Opt. **45**, 5582-5589 (2006).

5. J. Cariou, B. Le Jeune, J. Lotrian, and Y. Guern, “Polarization effects of seawater and underwater targets”, Appl. Opt. **29**, 1689-1695 (1990).
6. G. Le Brun, B. Le Jeune, J. Cariou, and J. Lotrian, “Laser imaging procedure for evaluating the polarization signature of immersed targets,” Pure Appl. Opt. **2**, 445-470 (1993).
7. P. Olivard, P. Y. Gerligand, B. Le Jeune, J. Cariou, and J. Lotrian, “Measurement of optical fibre parameters using an optical polarimeter and Stokes-Mueller formalism,” J. Phys. D : Appl. Phys. **32**, 1618-1625 (1999).
8. F. Bentivegna, , F. Boulvert, M. Guegan, B. Boulbry, A. Sharaiha, M. Tariaki, F. Pellen, B. Le Jeune, Y. Boucher, "Polarimetric analysis of a semiconductor optical amplifier based on the Mueller-Stokes formalism", *Sensors and Command, Control, Communications, and Intelligence (C3I) Technologies for Homeland Security and Homeland Defense III*, Proc SPIE, **5452**, 486-497 (2004)
9. V. Sankaran, J. T. Walsh Jr., and D. J. Maitland, “Comparative study of polarized light propagation in biological tissues”, J. Biomed. Opt. **7**, 300-306 (2002).
10. F. Boulvert, B. Boulbry, G. Le Brun, B. Le Jeune, S. Rivet, and J. Cariou, “Analysis of the depolarizing properties of irradiated pig skin,” J. Opt. A: Pure Appl. Opt. **7**, 21-28 (2005).
11. P. -Y. Gerligand, M. Smith, and R. Chipman, "Polarimetric images of a cone," Opt. Express **4**, 420-430 (1999).
12. O. Morel, C. Stolz, F. Meriaudeau, and P. Gorria, “Active lighting applied to three-dimensional reconstruction of specular metallic surfaces by polarization imaging,” Appl. Opt. **45**, 4062-4068 (2006).
13. P. J. Wu, and J. T. Walsh Jr., “Stokes polarimetry imaging of rat tail tissue in a turbid medium: degree of linear polarization image maps using incident linearly polarized light,” J. Biomed. Opt. **11**, 014031 (2006).
14. J. S. Tyo, and T. S. Turner Jr., “Variable-retardance, Fourier-transform imaging spectropolarimeters for visible spectrum remote sensing”, Appl. Opt. **40**, 1450-1458 (2001).
15. J. S. Tyo, D. L. Goldstein, D. B. Chenault, and J. A. Shaw, “Review of passive imaging polarimetry for remote sensing applications,” Appl. Opt. **45**, 5453-5469 (2006).
16. J. S. Tyo, “Noise equalization in Stokes parameter images obtained by use of variable-retardance polarimeters,” Opt. Lett. **25**, 1198-1200 (2000).
17. J. S. Tyo, “Design of optimal polarimeters: maximization of signal-to-noise ratio and minimization of systematic error,” Appl. Opt. **41**, 619-630 (2002).
18. D. H. Goldstein, and R. A. Chipman, “Error analysis of a Mueller matrix polarimeter,” J. Opt. Soc. Am. A **7**, 693-700 (1990).
19. B. Boulbry, B. Le Jeune, B. Bousquet, F. Pellen, J. Cariou, and J. Lotrian, “Error analysis and calibration of a spectroscopic Mueller matrix polarimeter using a short-pulse laser source,” Meas. Sci. Technol. **13**, 1563-1573 (2002).
20. G. H. Golub, and C. F. Van Loan, *Matrix Computations* (Johns Hopkins U. Press, Baltimore, Md) Chap. 2, 11-29 (1983).
21. W. H. Press, S. A. Teukolsky, W. T. Vetterling, and B. P. Flannery, *Numerical Recipes in C* (Cambridge University Press) Chap. 2, 59-71 (1992).
22. B. Boulbry, T. A. Germer, J. C. Ramella-Roman, "A novel hemispherical spectro-polarimetric scattering instrument for skin lesion imaging", *Photonic Therapeutics and Diagnostics II*, Proc. SPIE, **6078**, 128-134 (2006).
23. B. Laude-Boulesteix, A. De Martino, B. Drévillon, and L. Schwartz, “Mueller polarimetric imaging system with liquid crystals,” Appl. Opt. **43**, 2824-2832 (2004).
24. S. Huard, *Polarization of Light* (John Wiley & sons, 1997).
25. R. J. King, “Quarter-wave retardation systems based on the Fresnel rhomb principle,” J. Sci. Instrum. **43**, 617-622 (1966).